Journal of Materials Chemistry A

Accepted Manuscript

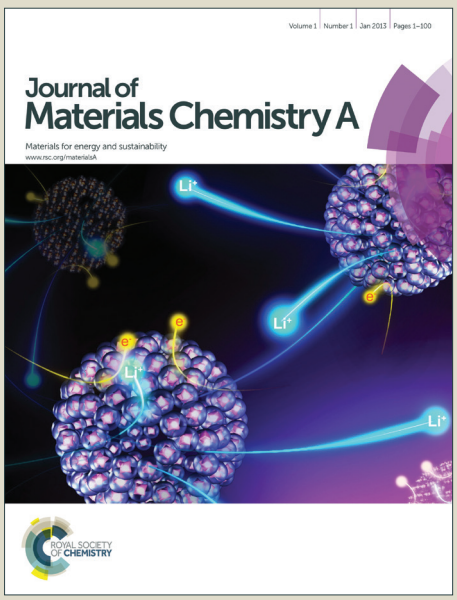

ROYAL SOCIETY OF CHEMISTRY

www.rsc.org/materialsA

Journal Name

ARTICLE

Controlled synthesis of V_2O_5/MWCNTs core/shell hybrid aerogels through a mixed growth and self–assembly methodology for supercapacitors with high capacitance and ultralong cycle life

Received 00th January 20xx,
Accepted 00th January 20xx

DOI: 10.1039/x0xx00000x

www.rsc.org/

Yingjie Wu, Guohua Gao,* Huiyu Yang, Wenchao Bi, Xin Liang, Yuerou Zhang, Guyu Zhang, and Guangming Wu*

Vanadium pentoxide (V_2O_5)/multiwalled carbon nanotubes (MWCNTs) core/shell hybrid aerogels with different MWCNTs content are controlled synthesized through a facile mixed growth and self–assembly methodology. V_2O_5 coated MWCNTs from the *in–situ* growth of V_2O_5 on the surface of acid–treated MWCNTs incorporate with V_2O_5 nanofibers from the preferred orientation growth of V_2O_5 in a one–step sol–gel process. These two kinds of one–dimensional fibers self–assemble into a three–dimensional monolithic porous hybrid aerogel. Owing to its high specific surface area, favorable electrical conductivity and unique three–dimensional and core/shell structures, the light weight hybrid aerogel (about 30 mg cm^{-3}) exhibits excellent specific capacitance (625 F g^{-1}), high energy density (86.8 Wh kg^{-1}) and outstanding cycle performance (> 20000 cycles). And the optimal content of MWCNTs in hybrid aerogels for highest–performance supercapacitor is 7.6%.

Introduction

Energy crisis has become one of increasingly serious global problems.[1] To meet the growing energy demands, electrochemical energy storage systems with high power and energy densities, good stability and low cost have been vigorously developed, such as lithium–ion batteries, lithium–air (O_2) and lithium–sulfur batteries, sodium–ion batteries and supercapacitors (electrochemical capacitors).[2–5] Because of its high power density, rapid charging/discharging rate and long cycle life, supercapacitor draws more and more attention.[6] The performance of supercapacitors is strongly dependent on the properties of electrode materials.[7] Carbon materials, conductive polymers and transition metal oxides are widely available to supercapacitors.[8–10] In recent years, vanadium pentoxide (V_2O_5) as one of promising candidate electrode materials in supercapacitors has attracted extensive attention due to its low cost, abundance and high potential pseudocapacitive characteristics (2120 F g^{-1}).[11–13] Up to now, a wide range of V_2O_5 materials with different structures and morphologies have been successively synthesized, including nanospheres, nanowires, nanotubes, nanobelts, nanosheets, aerogels, and so on.[14–19] However, the electrochemical performance of these V_2O_5 materials is still unsatisfied because of the poor ionic diffusivity (10^{-13}–10^{-12} cm^2 s^{-1}) and electrical conductivity (10^{-3}–10^{-2} S cm^{-1}) of V_2O_5 itself.[20]

Incorporating with highly electrical conductive materials such as carbonaceous materials and conductive polymers is one of the feasible methods to improve the electrochemical performance of V_2O_5 electrode materials.[21–24] For example, V_2O_5/graphene hybrid aerogel was synthesized in our previous works.[25] Compared with the specific capacitance (SC) of raw V_2O_5 (157 F g^{-1}) and V_2O_5 aerogel (233 F g^{-1}), the composite aerogel has enhanced specific capacitance (486 F g^{-1}). However, this value is still far from the theoretical SC of V_2O_5. As a one–dimensional (1D) carbon materials, carbon nanotubes (CNTs), with high electrical conductivity (> 100 S cm^{-1}), low density (about 0.5–2 g cm^{-3}) and large specific surface area (SSA) (100–1000 m^2 g^{-1}), is one of the perfect candidates.[26–28] To date, a lot of efforts have been spent on developing V_2O_5/CNTs composite electrode materials, such as V_2O_5–anchored CNTs,[29] V_2O_5 nanosheets assembled on CNTs,[30] V_2O_5 nanoparticles/CNTs hybrid films,[31] and intertwined V_2O_5 nanowire/CNTs nanocomposites.[32,33] Meanwhile, because of their one–dimensional (1D) or two–dimensional (2D) structures, the specific surface areas of these composites are relatively low, which is unfavorable for the improvement of the electrochemical performance of supercapacitors. On the other hand, three–dimensional (3D) MWCNTs/V_2O_5 core/shell sponge with high specific surface area can be synthesized through chemical vapor deposition (CVD) and atomic layer deposition (ALD) methods, but it requires severe conditions, sophisticated equipment and tedious procedures.[34] Until now, limited by its complex procedures, the controlled synthesis of

Shanghai Key Laboratory of Special Artificial Microstructure, School of Physics Science and Engineering, Tongji University, Shanghai, 200092, China. E–mail: gao@tongji.edu.cn; wugm@tongji.edu.cn.
Electronic Supplementary Information (ESI) available: [details of any supplementary information available should be included here]. See DOI: 10.1039/x0xx00000x

3D V_2O_5/CNTs composite electrode materials for high–performance supercapacitors still remains a challenge.

In search of an efficient and effective methodology to prepare 3D V_2O_5/CNTs composite electrode materials for enhanced supercapacitors, we introduce our work. In this study, we synthesized V_2O_5/multiwalled carbon nanotubes (MWCNTs) core/shell hybrid aerogels (VMA) through a facile mixed growth and self–assembly methodology in a mild one–pot sol–gel process. Due to its hierarchical porous structure, high specific surface area and good electrical conductivity, the VMA–based supercapacitors demonstrate extremely high specific capacitance, high power and energy densities, and excellent cycling stability. In addition, the MWCNTs content in the hybrid aerogels can be easily controlled and its effect on the electrochemical performance of supercapacitors was also characterized. Based on the systematic comparison analysis, the optimal content of MWCNTs in the VMA was also concluded.

Experimental

Synthesis of V_2O_5 sol

Functional V_2O_5 sol was prepared from commercial V_2O_5 powder. In a typical procedure, raw V_2O_5 powder, benzyl alcohol and isopropanol were mixed at a molar ratio of 1: 4: 40. Then the suspension was heated at 90 °C under condensate reflux for 4 h. After filtration, unreacted V_2O_5 was removed for recycling and the remainder pale yellow sol was concentrated to 1/3 volume through heating reflux. Thus, yellow functional V_2O_5 sol composed of vanadium oxide (VO_x) oligomers was obtained, in which V_2O_5 content was about 30 mg ml^{-1}.[25]

Fabrication of V_2O_5/MWCNTs core/shell hybrid aerogels

A certain concentration of mixed acid–treated (H_2SO_4: HNO_3 = 3: 1, volume ratio) MWCNTs aqueous dispersion (15 ml) was added into the V_2O_5 sol (10 ml) under vigorous stirring to induce hydrolysis of VO_x oligomers in V_2O_5 sol.[35] After about 10 min, VO_x/MWCNTs hybrid gel was obtained and then aged at 50 °C for 2 days. 3D VO_x/MWCNTs hybrid aerogel was obtained after solvent replacement and freeze drying process. Finally, crystalline VMA hybrid aerogel was successfully synthesized after thermal treatment in air at 300 °C for 3h. Moreover, to further determine and evaluate its influence on the electrochemical behavior of VMA, we adjusted the amount of MWCNTs through changing the concentration of its aqueous dispersion and hybrid aerogels with different MWCNTs content were easily synthesized. According to the mass (mg) of used MWCNTs, the hybrid aerogels were denoted as VMA–15, VMA–30, VMA–60 and VMA–120, respectively. For comparison, pure VO_x aerogel (V_xA) and V_2O_5 aerogel (VA) were also synthesized under the same conditions but without MWCNTs.

Characterizations

The morphologies and structures of the samples were systematically investigated by field emission scanning electron microscopy (FESEM, S–4800), transmission electron microscopy (TEM, JEOL–2100) and high–resolution transmission electron microscopy (HRTEM, field emission JEOL–2100). X–ray powder diffraction (XRD) pattern was obtained by using a RigakuD/max–C diffractometer with Cu Kα radiation source (λ = 1.5406 Å). X–ray photoelectron spectroscopy (XPS) experiments were carried out on a RBD upgraded PHI–5000C ESCA system (Perkin–Elmer) with Mg Kα radiation (hv = 1253.6 eV). The Differential Scanning Calorimetry (DSC) and thermogravimetry analysis (TGA) were carried out on a SDT Q600 over the temperature range from 50 to 750 °C at a heating rate of 10 °C min^{-1} under air flow. Raman spectra (Jobin–Yvon HR800) was recorded from 100 to 2000 cm^{-1} using a 514 nm argon ion laser. Nitrogen adsorption isotherms for calculating the Brunauer–Emmett–Teller (BET) surface area were measured using an Autosorb–1 (Quantachorme) analyzer. The compressive modulus (E_c) of aerogel was measured by an electronic universal tensile testing machine (CMT5105). The bulk electrical conductivity of hybrid aerogel was tested in a two–probe system: The obtained cylindrical aerogels without any manufacture were sandwiched between two copper foils and connected to a CHI 660C electrochemical workstation at room temperature.[36] The bulk electrical conductivity (κ, S m^{-1}) of aerogel was calculated via the formula $\kappa = 1/\rho = 4h/(\pi Rd^2)$, where ρ (Ω m), R (Ω), d (m) and h (m) were the electrical resistivity, resistance, diameter and height of synthesized cylindrical aerogel, respectively.

Electrochemical measurements

A symmetric two–electrode system with a 1 M Na_2SO_4 aqueous solution electrolyte was used to evaluate the electrochemical behavior of as–prepared electrode materials. The electrode was prepared by mixing 80% of the active materials, 10% acetylene black and 10% poly (vinylidene fluoride) (PVDF) dispersed in N–methylpyrrolidinone (NMP). The obtained mixed slurry (about 1 mg) was coated onto graphite papers (1 cm × 3 cm) with an area of 1 cm^2 and then the electrode was dried at 120 °C for 12 h under vacuum to remove the solvent. The cyclic voltammetry (CV) and galvanostatic charge/discharge measurements were carried out by a CHI 660C electrochemical workstation over the potential range from –1 to 1 V.[12] Electrochemical impedance spectroscopy (EIS) measurements were measured in a frequency range of 0.01 Hz to 100 kHz with AC amplitude of 5 mV by using CHI 660C electrochemical workstation. The specific capacitance for a single electrode (C_{single}, F g^{-1}) was calculated from the galvanostatic discharge curves as $C_{single} = 2I\Delta t/\Delta V$, where I is the constant discharging current density

based on the total mass of a single electrode, Δt is the discharging time and ΔV is the potential window, respectively. The energy density (E, Wh kg^{-1}) and average power density (P_{avg}, W kg^{-1}) of the device in Ragone plots were calculated by using the formula $E = (1/8)C_{single}(\Delta V)^2/3600$ and $P_{avg} = E/\Delta t$, respectively.[37]

Results and discussion

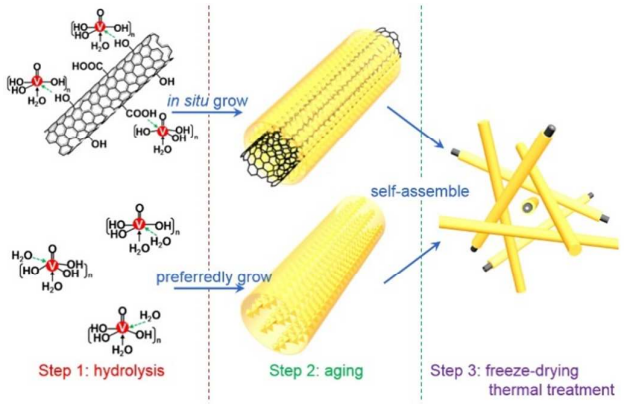

Fig. 1 Illustration of the mixed growth and self–assembly methodology for controlled synthesis of 3D V_2O_5/MWCNTs core/shell hybrid aerogels.

Three–dimensional (3D) V_2O_5/MWCNTs core/shell hybrid aerogels with different MWCNTs content were built from an efficient and effective mixed growth and self–assembly methodology. A certain concentration of mixed acid–treated MWCNTs aqueous dispersion was added into the V_2O_5 sol under vigorous stirring to induce hydrolysis of vanadium oxide (VO_x) oligomers in V_2O_5 sol. As described in Fig. 1, when the VO_x oligomers hydrolyse, vanadium exhibits a six–fold coordination with one H_2O molecule opposite the V=O double bond and an –OH group in the equatorial plane.[38] Some VO_x oligomers coordinate with –OH or –COOH on the surface of acid–treated MWCNTs, and these coordination bonds anchor the VO_x oligomers on MWCNTs.[29, 39, 40] Then VO_x oligomers condense rapidly and *in situ* grow along MWCNTs, yielding V_2O_5 coated MWCNTs. Simultaneously, the other VO_x oligomers coordinate with –OH in H_2O molecules, just like conventional hydrolysis procedure of V_2O_5.[41] After olation and oxolation process, fibrous V_2O_5 are obtained through preferred orientation growth. During aging extension, V_2O_5 coated MWCNTs and V_2O_5 nanofibers fully grow and gradually interconnect with each other. Finally, the two kinds of 1D nanowires self–assemble into a monolithic 3D architecture. After freeze drying and thermal treatment process, the ideal 3D porous structure is completely retained. Thus, a V_2O_5/MWCNTs core/shell hybrid aerogel is successfully constructed through a facile mixed growth and self–assembly methodology. Moreover, to further determine and evaluate its influence on the electrochemical behavior of VMA, we adjusted the amount of MWCNTs through changing the concentration of its aqueous dispersion, and hybrid aerogels with different MWCNTs content were controlled synthesized. The digital photographs of as–prepared aerogels are displayed in Fig. S1 in ESI. There are two reasons for acid treatment of MWCNTs in our method: (i) homogeneous and stable aqueous dispersion prepared from acid–treated MWCNTs is the prerequisite for uniform 3D architecture; (ii) the abundant functional groups on the surface of acid–treated MWCNTs make it highly active in capture VO_x oligomers, which makes sure the formation of core/shell structures in *in–situ* growth step.

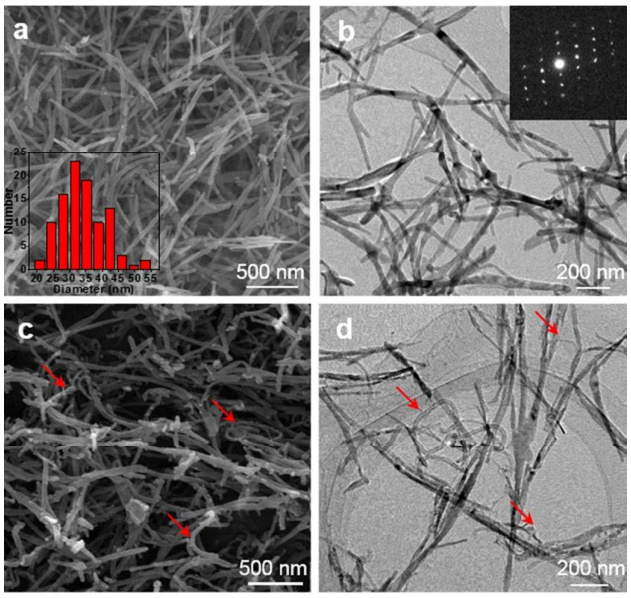

Fig. 2 (a) SEM image of V_2O_5 aerogel and diameter distribution of V_2O_5 nanofibers (inset); (b) TEM image of V_2O_5 aerogel and SAED patterns of V_2O_5 nanofibers (inset); (c, d) SEM and TEM images of VMA–120 hybrid aerogel. Curled MWCNTs are pointed out by red arrows and detailed SEM and TEM images of MWCNTs, VMA–15, VMA–30 and VMA–60 are displayed in Fig. S5 in ESI.

The microstructures of synthesized aerogels are investigated by scanning electron microscopy (SEM), transmission electron microscopy (TEM), and high resolution transmission electron microscopy (HRTEM). As shown in Figs. 2a and 2b, 3D pure V_2O_5 aerogel is composed of intersectional randomly arranged V_2O_5 nanofibers. The SAED patterns and XRD results of VO_x and V_2O_5 aerogel (Figs. 2b, S2 and S3 in ESI) indicate that V_2O_5 nanofibers crystallized after thermal treatment. Similar results can also be obtained from thermogravimetric curve of VO_x aerogel (Fig. S4a). These V_2O_5 nanofibers are several micrometres long, with an average diameter of 33.8 nm (inset in Fig. 2a). The morphology of these fibers are nearly straight due to their crystalline structure, which makes it easy to distinguish them from the curled MWCNTs in hybrid aerogels. Figs. 2c and 2d confirm that V_2O_5 nanofibers combine with MWCNTs and obtained V_2O_5/MWCNTs hybrid aerogels exhibit similar 3D structures even after thermal treatment at 300 °C (for details, see Fig. S5 in ESI). The elemental mapping of hybrid aerogels (Fig. S6 in ESI) displays a uniform mixture of

V_2O_5 and MWCNTs in composite materials. That is mainly caused by the favorable dispersity of acid–treated MWCNTs in water.[42]

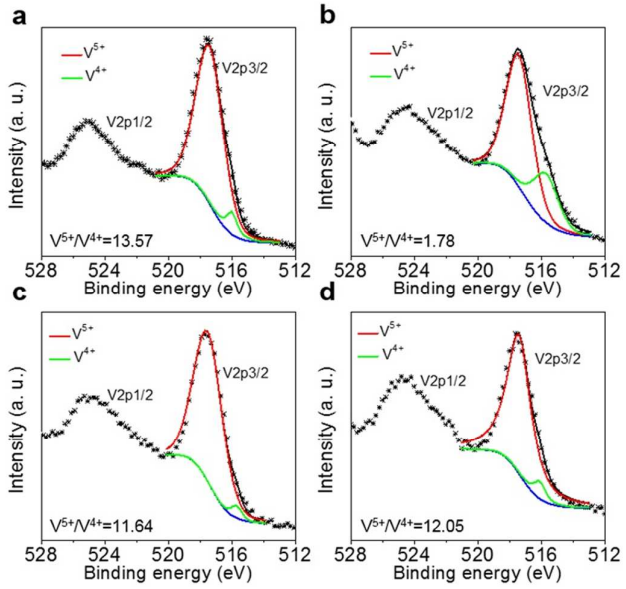

Fig. 3 XPS spectra of V2p3/2 and V2p1/2 in (a) raw V_2O_5, (b) VO_x aerogel, (c) V_2O_5 aerogel and (d) VMA–120 hybrid aerogel. See Fig. S7 for XPS spectra of VMA–15, VMA–30 and VMA–60 hybrid aerogels.

In addition, X–ray photoelectron spectroscopy (XPS) measurement was applied to investigate the valence change of vanadium in synthesis process.[43] As shown in Figs. 3 and S7, the transformation from VO_x to V_2O_5 during thermal treatment is confirmed through compare the ratio of V^{5+} peak area to V^{4+} peak area under XPS spectra of raw V_2O_5, VO_x aerogel, V_2O_5 aerogel and V_2O_5/MWCNTs hybrid aerogels. The ratio of V^{5+}/V^{4+} for VO_x aerogel (1.78) is much lower than raw V_2O_5 (13.57), which confirms the existence of abundant V^{4+} in VO_x aerogel. After thermal treatment, the ratio of V^{5+}/V^{4+} for V_2O_5 aerogel is 11.64, indicating that V^{4+} is oxidized to V^{5+} by O_2 during thermal treatment at 300 °C in air. Same results can also be concluded in VMA hybrid aerogels, indicating that the vanadium in VMA hybrid aerogel is mainly composed of V_2O_5. The incorporation of V_2O_5 and MWCNTs in hybrid aerogels is further verified through comparing the Raman spectra of MWCNTs, pure V_2O_5 aerogel and hybrid aerogels. As shown in Fig. 4, there are six peaks at 140, 282, 406, 518, 688 and 993 cm^{-1} for V_2O_5/MWCNTs hybrid aerogels corresponding to the skeleton bending vibration of the V–O–V bonds, bending vibration of V=O bonds, bending vibration of bridge oxygen bonds, stretching vibration of triply coordinated oxygen bonds, stretching vibration of doubly coordinated oxygen and in–phase stretching vibrational of V=O bonds, respectively.[44] Notably, the characteristic peaks of the D and G bands of MWCNTs at 1349 and 1577 cm^{-1} are also detected in hybrid aerogels and their relative peak intensities are increased with the increase of MWCNTs content.[42] Thus, the incorporation of V_2O_5 with MWCNTs and the different MWCNTs content in hybrid aerogel are proved simultaneously.

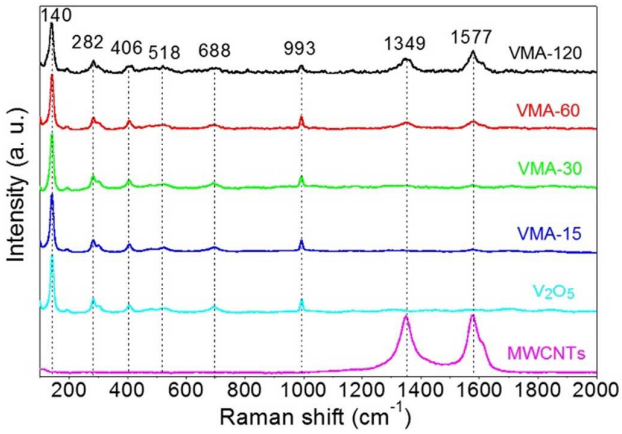

Fig. 4 Raman spectra of MWCNTs, raw V_2O_5 and V_2O_5/MWCNTs hybrid aerogels.

To further investigate the core/shell structure of V_2O_5 coated MWCNTs, we focused on the individual MWCNTs. As shown in Fig. 5a, the outer diameter of naked tubular MWCNTs is about 25 nm. During hydrolysis process, V_2O_5 *in situ* grows on the surface of acid–treated MWCNTs, forming a double–layer tubular core/shell structure (Fig. 5b). The thickness of V_2O_5 coating layer is ranging from 5 nm to 13 nm (Fig. 5c). As shown in Figs. 5d–g, the high–angle annular diffraction–scanning transmission electron microscopy (HAADF–STEM) image and corresponding element mappings of vanadium, oxygen and carbon in V_2O_5 coated MWCNTs intuitively conform its core/shell microstructure.

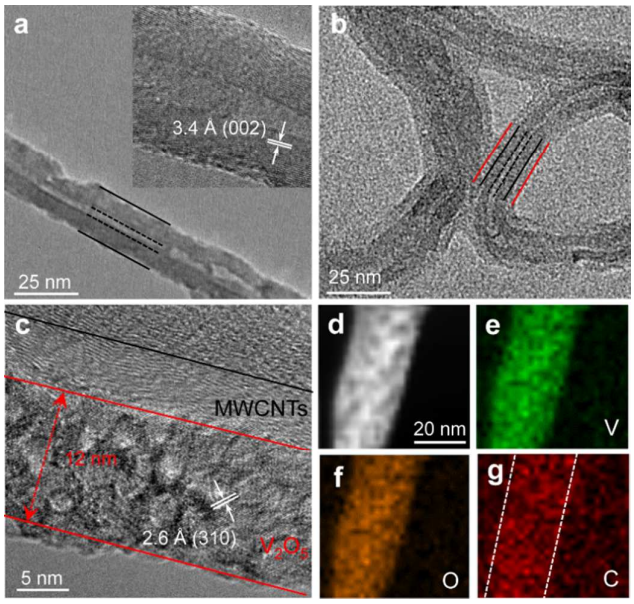

Fig. 5 (a) HRTEM image of naked MWCNTs; (b, c) HRTEM images of V_2O_5 coated MWCNTs; (d) HAADF–STEM image of V_2O_5/MWCNTs core/shell nanowire and corresponding elemental mapping images of (e) vanadium, (f) oxygen and (g) carbon.

It is worth noting that different from 1D V_2O_5 coated MWCNTs nanowires or 2D V_2O_5/MWCNTs intertwined

composite firms, our synthesized V_2O_5/MWCNTs core/shell hybrid aerogels exhibit unique uniform 3D porous frameworks, which is benefiting from the good dispersibility of acid treated MWCNTs, mild sol–gel reaction and freeze drying process. As summarized in Table 1, the obtained V_2O_5/MWCNTs core/shell composite aerogels are extraordinary light. With different content of MWCNTs, their densities are ranging from 26 to 30 mg cm^{-3}, which are quite lighter than other metal based aerogels, such as Al_2O_3 aerogel (93 mg cm^{-3}), CuO aerogel (267 mg cm^{-3}), TiO_2 aerogel (145 mg cm^{-3}), ZrO_2 aerogel (446 mg cm^{-3}), Mo aerogel (150 mg cm^{-3}) and Cr aerogel (230 mg cm^{-3}).[45–49] Many metal aerogels are notably weak and fragile in monolithic form. In particular, it is especially difficult to prepare uncracked, robust and stable metal aerogels with densities less than 30 mg cm^{-3}.[50] Supported by the strong V_2O_5 nanofibers, the skeleton structure of our V_2O_5 aerogel is very sturdy, with no crack and shrinkage after freeze–drying process. According to the decrease of compress modulus (E_c) of hybrid aerogels in Table 1, it can also be concluded that incorporating with flexible MWCNTs can further reduce the compressive modulus of aerogel, partly overcome the brittleness of 3D V_2O_5 architecture and improve its mechanical characteristics, which is conductive to mass production, further processing and application. In addition, owning to the high electrical conductivity of MWCNTs, the bulk electrical conductivity of synthesized aerogels are improved when the MWCNTs content was increased. Notably, due to its robust 3D porous structure, low density and high specific surface area of added MWCNTs (147 m^2 g^{-1}), VMA has a large specific surface area even after thermal treatment at 300 °C (Table 1). Besides, our 3D hybrid aerogels exhibit typical hierarchical macro–, meso–, and microporous structures, the nitrogen adsorption–desorption isotherms and Barrett–Joyner–Halenda (BJH) pore–size distributions of hybrid aerogel are concluded in Fig. S8 in ESI. These abundance porous structure can afford enough adsorption sites and facilitate the ion diffusion in electrochemical process.

The unique hierarchical porous structure, high specific surface area and excellent electrical conductivity of the V_2O_5/MWCNTs hybrid aerogel render it an excellent candidate in electrode materials of supercapacitors. As evidence, we analyzed the electrochemical behavior of the as–prepared hybrid aerogels in a symmetric two–electrode system with a 1 M Na_2SO_4 aqueous solution as electrolyte. As shown in Fig. 6a, the nearly rectangular cyclic voltammetry (CV) curve of VMA–30 exhibits largest area and typical characteristics of electrochemical double layer capacitors (EDLCs) and pseudocapacitors. In agreement with the conclusion of CV curves, the specific capacitance derived from galvanostatic charge/discharge curves (Figs. 6b and S9 in ESI) at 0.5 A g^{-1} of V_2O_5/MWCNTs hybrid aerogel (625 F g^{-1} for VMA–30) is much higher than raw V_2O_5 powder (156.5 F g^{-1} at 0.5 A g^{-1}), pure V_2O_5 aerogel (223 F g^{-1} at 0.5 A g^{-1}), MWCNTs (147 F g^{-1} at 0.5 A g^{-1}), interconnected V_2O_5 nanoporous network (304 F g^{-1} at 0.1 A g^{-1}),[51] 3D V_2O_5 nanosheets (451 F g^{-1} at 0.1 A g^{-1}),[12] interpenetrating V_2O_5/CNTs networks (440 F g^{-1} at 0.25 A g^{-1}),[52] V_2O_5/graphene hybrid aerogel (486 F g^{-1} at 0.5 A g^{-1}).[25] To further explore the reason of the high capacitance of our hybrid aerogel and the relationship of MWCNTs with the electrochemical performance of VMA, we systematically tested the CV and galvanostatic charge/discharge curves of VMA with different content of MWCNTs, and the results are shown in Figs. 6c and S10 in ESI. The specific capacitances at 0.5 A g^{-1} of VMA–15, VMA–30, VMA–60 and VMA–120 are 410, 625, 356 and 279 F g^{-1}, respectively.

Consistent with the results of Chen *et al*, the effect of MWCNTs content on the electrochemical performance of composite materials is not in linearity.[52] According to our experiment, the specific capacitance of VMA hits its peak of 625 F g^{-1} when the content of MWCNTs is 7.6% (VMA–30). To elucidate the mechanism of this affection, the charge transfer resistance (R_{ct}) of as–prepared aerogels are compared via the electrochemical impedance spectroscopy (EIS) measurements (see Fig. S11 and Table S1 in ESI for more details). As shown in Fig. 6d, the R_{ct} of V_2O_5 aerogel (5.87 Ω) is much lower than raw V_2O_5 powder (49.33 Ω). It is mainly due to the homogeneous 3D structure and high SSA of VA, which can minimize the diffusion distance of electrolytes to interior surfaces.[53] In addition, MWCNTs can further decrease the resistance of V_2O_5 aerogel, and the R_{ct} of VMA–15, VMA–30, VMA–60 and VMA–120 are 3.22, 2.28, 2.27 and 1.99 Ω, respectively. From above results, we can conclude that: when the content of MWCNTs in VMA is less than 7.6% (VMA–30), electrical conductivity is the major limitation in the electrochemical performance of hybrid

Table 1 Physical characteristics of synthesized aerogels

Aerogels	MWCNTs[a] [%]	Density[b] [mg cm^{-3}]	Compress modulus [MPa]	Bulk electrical conductivity [mS cm^{-1}]	Specific surface area [m^2 g^{-1}]
VA	0	26.11	0.38	0.66	35
VMA–15	4.3	28.58	0.22	0.87	61
VMA–30	7.6	28.43	0.20	0.91	103
VMA–60	11.2	27.30	0.12	1.02	146
VMA–120	31.8	29.97	0.08	1.39	163

[a] The contents of MWCNTs in hybrid aerogel were calculated according to their TG curves (Fig S4b). [b] The densities of synthesized aerogels were calculated according to the ratio of their mass and volume.

aerogels; Meanwhile, once the MWCNTs content is higher than 7.6%, the electrical conductivity of VMA is as good as individual MWCNTs (1.80 Ω), and the SC of VMA is mainly attributed to the pseudocapacitors of V_2O_5. Since specific surface area plays an important role in the adsorption–desorption process in EDLCs, the influence of SSA on the specific capacitance of hybrid aerogels must also be taken into account. However, the contribution of EDLCs by improving the specific surface area is much smaller than pseudocapacitors owing to V_2O_5. And the V_2O_5 content in VMA–30 is highest among the same mass of electrode materials prepared from VMA–30, VMA–60 and VMA–120. This is the reason why VMA–30 exhibits highest specific capacitance among these hybrid aerogels.

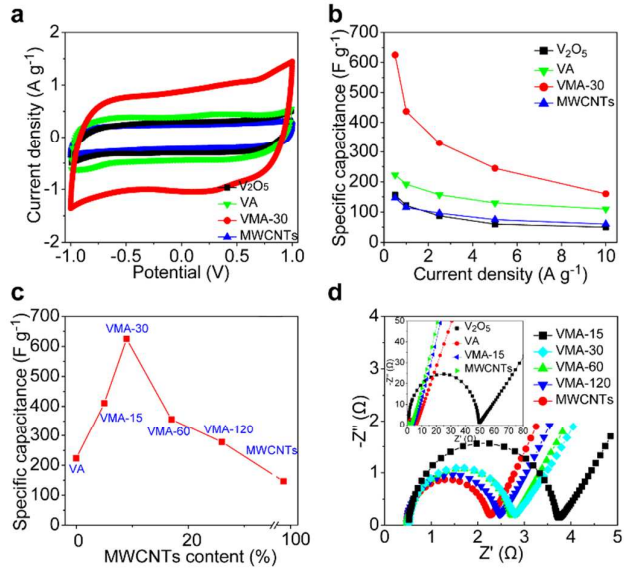

Fig. 6 (a) CV curves of raw V_2O_5 powder, MWCNTs, V_2O_5 aerogel and VMA–30 hybrid aerogel at a scan rate of 5 mV s^{-1}; (b) Specific capacitance as a function of current density for raw V_2O_5 powder, MWCNTs, V_2O_5 aerogel and VMA–30 hybrid aerogel; (c) Specific capacitances of hybrid aerogels with different MWCNTs content; (d) EIS spectra of raw V_2O_5 powder, V_2O_5 aerogel, V_2O_5/MWCNTs hybrid aerogels and MWCNTs.

Difference is worth noting that the SC of V_2O_5/MWCNTs intertwined composites reaches peak when the content of MWCNTs is about 35%,[52] whereas the best amount of MWCNTs in our hybrid aerogel is 7.6%. It is partly because of the good electrical conductivity of original V_2O_5 aerogel itself, but more importantly because of the unique core/shell structures of V_2O_5 coated MWCNTs. In addition, to evaluate the attribution of core/shell structure to the improvement of the specific capacitance of supercapacitors, we prepared V_2O_5 aerogel/MWCNTs composite through simply mixing V_2O_5 aerogel and MWCNTs. The content of MWCNTs in the composite material was 7.6%. And for convenience of comparing, the composite was denoted as VMC−30. As shown in Fig. 7a and S11, the specific capacitance of VMC−30 composite (356.5 F g^{-1}, 0.5 A g^{-1}) is much lower than VMA−30 hybrid aerogel. It is because that the core/shell structure can significantly shorten the charge transfer distance and reduce the charge transfer resistance (from 4.82 to 2.28 Ω) between V_2O_5 and MWCNTs (Fig. 7b and Table S1). Thus, the role of MWCNTs and V_2O_5 in the hybrid aerogel is clear: MWCNTs is in charge of reducing the electrical conductivity of VMA and providing smooth pathways for electron transfer; V_2O_5 contributes to the pseudocapacitors through Faradic reactions.

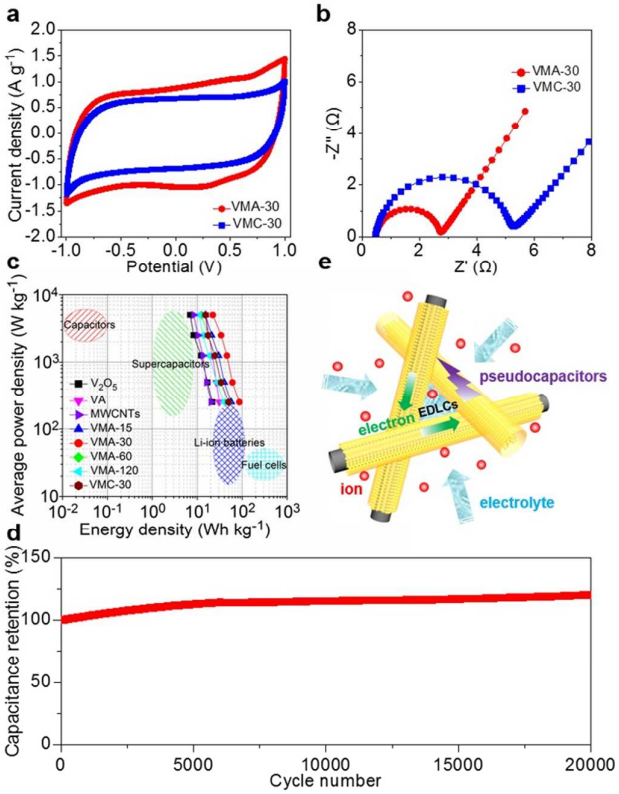

Fig. 7 (a) CV curves of VMA–30 hybrid aerogel and VMC–30 composite at a scan rate of 5 mV s^{-1}; (b) EIS spectra of VMA–30 hybrid aerogel and VMC–30 composite; (c) Ragone plots of supercapacitors based on V_2O_5 powder, V_2O_5 aerogel, MWCNTs, V_2O_5/MWCNTs hybrid aerogels and VMC–30 composite material; (d) Cycling performance of supercapacitor with VMA–30 electrodes at a large current density of 10 A g^{-1}; (e) Schematic of electrochemical behavior in hybrid aerogels.

Fig. 7c compares the energy density and power density of different prototype supercapacitors. Notably, the VMA–30 exhibits a highest energy density of 86.8 Wh kg^{-1} at an average power density of 250 W kg^{-1}, which bridges the gap between supercapacitors and Li–ion batteries. As shown in Fig. 7d, the SC of VMA–30 gradually increases in first 5000 charge/discharge recycles at a large current density of 10 A g^{-1}, which is owing to the improvement of surface wetting between the electrode materials and the electrolyte during the cycling and the electroactivation process.[54] The capacitance retention of VMA–30 stabilizes around 120% even after 20000 circulations, indicating the excellent cycling

stability of hybrid aerogel. As concluded in Fig. 7e, the enhanced specific capacitance, high energy and power densities and extremely long cycle life of VMA–based supercapacitors are owing to: (i) 3D hierarchical porous structure and high specific surface area of hybrid aerogels, which provide multidimensional electron transport pathways and shorten the transport distances of electrolyte; (ii) synergistic effect of the EDLCs and pseudocapacitors, which increases specific capacitance and cycling stability of supercapacitors simultaneously; and (iii) the core/shell structure of V_2O_5 coated MWCNTs and excellent electrical conductivity of hybrid aerogels, which further minimizes the charge transfer distance and reduces the charge transfer resistance.[55–57]

Conclusions

In summary, we controlled synthesized V_2O_5/MWCNTs core/shell hybrid aerogels with different MWCNTs content through a facile mixed growth and self–assembly methodology in a sol–gel process. During hydrolysis process, core/shell structure V_2O_5 coated MWCNTs and V_2O_5 nanowires were obtained simultaneously through *in–situ* growth and preferred orientation growth, respectively. Then these two kinds of 1D nanowires self–assembled into 3D V_2O_5/MWCNTs hybrid aerogels. Due to its unique core/shell structure, high specific area, low resistance, and synergistic action of EDLCs and pseudocapacitors, the hybrid aerogels exhibits excellent electrochemical performance with high specific capacitance (625 F g^{-1}), high energy density (86.8 Wh kg^{-1}) and extremely outstanding cycle stability (> 20000). Because of the competitive effect of electrical conductivity (MWCNTs) and pseudocapacitors (V_2O_5) in the electrochemical behavior of hybrid aerogels, the optimum content of MWCNTs in hybrid aerogel for highest–performance supercapacitor is 7.6%. Based on the above results, we believe that the V_2O_5/MWCNTs core/shell hybrid aerogels can be used in broader applications, such as Li–ion batteries, sensors, electronics, catalysts and adsorbents. Besides, these V_2O_5/MWCNTs core/shell hybrid aerogels show a novel structure of V_2O_5/MWCNTs composites. And it may become possible to build other 3D V_2O_5/carbonaceous materials composites through our mixed growth and self–assembly methodology, such as V_2O_5/active carbon, V_2O_5/carbon aerogel and V_2O_5/carbon fiber composites.

Acknowledgements

The authors gratefully acknowledge the financial support from Fundamental Research Funds for the Central Universities, the Shanghai Committee of Science and Technology (11nm0501300 and 13JC1408700), the National Natural Science Foundation of China (51472182, 51272179 and 51102183) and the National High–Tech R–D Program of China (863 Program) (2013AA031801).

Notes and references

1 S. Chu and A. Majumdar, *Nature*, 2012, **488**, 294.
2 A. Manthiram, *J. Phys. Chem. Lett.*, 2011, **2** 176.
3 P. G. Bruce, S. A. Freunberger, L. J. Hardwick and J. M. Tarascon, *Nat. Mater.*, 2012, **11**, 19.
4 V. Palomares, P. Serras, I. Villaluenga, K. B. Hueso, J. Carretero–González and T. Rojo, *Energy Environ. Sci.*, 2012, **5**, 5884.
5 B. E. Conway, Electrochemical supercapacitor: Scientific Fundamentals and Technological Applications, Kluwer Academic/Plenum Publisher, New York, 1999.
6 Y. G. Wang and Y. Y. Xia, *Adv. Mater.*, 2013, **25**, 5336.
7 P. Simon and Y. Gogotsi, *Nat. Mater.*, 2008, **7**, 845.
8 L. L. Zhang and X. S. Zhao, *Chem. Soc. Rev.*, 2009, **38**, 2520.
9 G. A. Snook, P. Kao and A. S. Best, *J. Power Sources*, 2011, **196**, 1.
10 C. Z. Yuan, H. B. Wu, Y. Xie and X. W. Lou, *Angew. Chem. Int. Ed.*, 2014, **53**, 1488.
11 M. J. Zhi, C. C. Xiang, J. T. Li, M. Li and N. Q. Wu, *Nanoscale*, 2013, **5**, 72.
12 J. X. Zhu, L. J. Cao, Y. S. Wu, Y. J. Gong, Z. Liu, H. E. Hoster, Y. H. Zhang, S. T. Zhang, S. B. Yang, Q. Y. Yan, P. M. Ajayan and R. Vajtai, *Nano Lett.*, 2013, **13**, 5408.
13 G. Wee, H. Z. Soh, Y. L. Cheah, S. G. Mhaisalkar and M. Srinivasan, *J. Mater. Chem.*, 2010, **20**, 6720.
14 A. M. Cao, J. S. Hu, H. P. Liang and L. J. Wan, *Angew. Chem. Int. Ed.*, 2005, **44**, 4391.
15 T. Y. Zhai, H. M. Liu, H. Q. Li, X. S. Fang, M. Y. Liao, L. Li, H. S. Zhou, Y. Koide, Y. Bando and D. Golberg, *Adv. Mater.*, 2010, **22**, 2547.
16 X. W. Zhou, G. M. Wu, G. H. Gao, J. C. Wang, H. Y. Yang, J. D. Wu, J. Shen, B. Zhou and Z. H. Zhang, *J. Phys. Chem. C*, 2012 **116**, 21685.
17 J. F. Liu, X. Wang, Q. Peng and Y. D. Li, *Adv. Mater.*, 2005, **17**, 764.
18 X. H. Rui, Z. Y. Lu, Z. Y. Yin, D. H. Sim, N. Xiao, T. M. Lim, H. H. Hng, H. Zhang and Q. Y. Yan, *Small*, 2013, **9**, 716.
19 A. Moretti, F. Maroni, I. Osada, F. Nobili and S. Passerini, *ChemElectroChem*, 2015, **2**, 529.
20 K. Takahashi, Y. Wang and G. Z. Cao, *J. Phys. Chem. B*, 2005, **109**, 48.
21 Q. Liu, Z. F. Li, Y. D. Liu, H. Y. Zhang, Y. Ren, C. J. Sun, W. Q. Lu, Y. Zhou, L. Stanciu, E. A. Stach and J. Xie. *Nat. Commun.*, 2015, **6**, 6127.
22 V. Raju, J. Rains, C. Gates, W. Luo, X. F. Wang, W. F. Stickle, G. D. Stucky and X. L. Ji, *Nano Lett.*, 2014, **14**, 4119.
23 D. Chao, X. Xia, J. Liu, Z. Fan, C. F. Ng, J. Lin, H. Zhang, Z. X. Shen and H. J. Fan, *Adv. Mater.*, 2014, **26**, 5794.
24 L. Q. Mai, F. Dong, X. Xu, Y. Z. Luo, Q. Y. An, Y. L. Zhao, J. Pan and J. N. Yang, *Nano Lett.*, 2013, **13**,740.
25 Y. J. Wu, G. H. Gao and G. M. Wu, *J. Mater. Chem. A*, 2015, **3**, 1828.
26 T. W. Ebbesen, H. J. Lezec, H. Hiura, J. W. Bennett, H. F. Ghaemi and T. Thio, *Nature*, 1996, **382**, 54.
27 R. R. Bacsa, C. Laurent, A. Peigney, W. S. Bacsa, T. Vaugien and A. Rousset, *Chem. Phys. Lett.*, 2000, **323**, 566.
28 R. H. Baughman, A. A. Zakhidov and W. A. de Heer, *Science*, 2002, **297**, 787.
29 M. Sathiya, A. S. Prakash, K. Ramesha, J. M. Tarascon and A. K. Shukla, *J. Am. Chem. Soc.*, 2011, **133**, 16291.
30 R. X. Yu, C. F. Zhang, Q. Meng, Z. X. Chen, H. K. Liu and Z. P. Guo, *ACS Appl. Mater. Interfaces*, 2013, **5**, 12394.
31 Z. Y. Cao and B. Q. Wei, *Nano Energy*, 2013, **2**, 481.
32 S. D. Perera, B. Patel, N. Nijem, K. Roodenko, O. Seitz, J. P. Ferraris, Y. J. Chabal and K. J. Balkus Jr, *Adv. Energy Mater.*, 2011, **1**, 936.

33 Z. Chen, V. Augustyn, J. Wen, Y. W. Zhang, M. Q. Shen, B. Dunn and Y. F. Lu, *Adv. Mater.*, 2011, **23**, 791.
34 X. Y. Chen, H. L. Zhu, Y. C. Chen, Y. Y. Shang, A. Y. Cao, L. B. Hu and G. W. Rubloff, *ACS Nano*, 2012, **6**, 7948.
35 K. A. Wepasnick, B. A. Smith, K. E. Schrote, H. K. Wilson ,S. R. Diegelmann and D. H. Fairbrother, *Carbon*, 2011, **49**, 24.
36 Y. X. Xu, K. X. Sheng, C. Li and G. Q. Shi, *ACS Nano*, 2010, **4**, 4324.
37 X. B. Wang, Y. J. Zhang, C. Y. Zhi, X. Wang, D. M. Tang, Y. B. Xu, Q. H. Weng, X. F. Jiang, M. Mitome, D. Golberg and Yoshio Bando, *Nat. Commun.*, 2013, **4**, 2905.
38 J. Livage, *Chem. Mater.*, 1991, **3**, 578.
39 Q. Liu, Z. F. Li, Y. D. Liu, H. Y. Zhang, Y. Ren, C. J. Sun, W. Q. Lu, Y. Zhou, L. Stanciu, E. A. Stach and J. Xie, *Nat. Commun.*, 2015, **6**, 6127.
40 H. Zhang, A. J. Xie, C. P. Wang, H. S. Wang, Y. H. Shen and X. Y. Tian, *ChemPhysChem*, 2014, **15**, 366.
41 J. Livage, *Solid State Ionics*, 1996, **86**, 935.
42 V. Datsyuk, M. Kalyva, K. Papagelis, J. Parthenios, D. Tasis, A. Siokou, I. Kallitsis and C. Galiotis, *Carbon*, 2008, **46**, 833.
43 I. E. Rauda, V. Augustyn, L. C. Saldarriaga–Lopez, X. Y. Chen, L. T. Schelhas, G. W. Rubloff, B. Dunn and S. H. Tolbert, *Adv. Funct. Mater.*, 2014, **24**, 6717.
44 B. Yan, L. Liao, Y. M. You, X. J. Xu, Z. Zheng, Z. X. Shen, Jan Ma, L. M. Tong and T. Yu, *Adv. Mater.*, 2009, **21**, 2436.
45 G. Q. Zu, J. Shen, L. P. Zou, W. Q. Wang, Y. Lian, Z. H. Zhang and A. Du, *Chem. Mater.*, 2013, **25**, 4757.
46 A. Du, B. Zhou, J. Shen, S. F. Xiao, Z. H. Zhang, C. Z. Liu and M. X. Zhang, *J. Non–Cryst. Solids*, 2009, **355**, 175.
47 G. Q. Zu, J. Shen, W. Q. Wang, L. P. Zou, Y. Lian, Z. H. Zhang, B. Liu and F. Zhang, *Chem. Mater.*, 2014, **26**, 5761.
48 A. Du, B. Zhou, Y. H. Zhong, X. R. Zhu, G. H. Gao, G. M. Wu, Z. H. Zhang and J. Shen, *J. Sol–Gel Sci. Technol.*, 2011, **58**, 225.
49 A. Du, B. Zhou, J. Shen, J. Y. Gui, Y. H. Zhong, C. Z. Liu, Z. H. Zhang and G. M. Wu, *New J. Chem.*, 2011, **35**, 1096.
50 J. F. Poco, J. H. Satcher Jr and L. W. Hrubesh, *J. Non–Cryst. Solids*, 2001, **285**, 57.
51 B. Saravanakumar, K. K. Purushothaman and G. Muralidharan, *ACS Appl. Mater. Interfaces*, 2012, **4**, 4484.
52 Z. Chen, Y. C. Qin, D. Weng, Q. F. Xiao, Y. T. Peng, X. L. Wang, H. X. Li, F. Wei and Y. F. Lu, *Adv. Funct. Mater.*, 2009, **19**, 3420.
53 Z. S. Wu, Y. Sun, Y. Z. Tan, S. B. Yang, X. L. Feng and K. Müllen, *J. Am. Chem. Soc.*, 2012, **134**, 19532.
54 Y. F. Yan, Q. L. Cheng, Z. J. Zhu, V. Pavlinek, P. Saha and C. Z. Li, *J. Power Sources*, 2013, **240**, 544.
55 D. W. Wang, F. Li, M. Liu, G. Q. Lu and H. M. Cheng, *Angew. Chem. Int. Ed.*, 2008, **47**, 373.
56 Z. S. Wu, A. Winter, L. Chen, Y. Sun, A. Turchanin, X. L. Feng and K. Müllen, *Adv. Mater.*, 2012, **24**, 5130.
57 F. X. Wang, S. Y. Xiao, Y. Y. Hou, C. L. Hu, L. L. Liu and Y. P. Wu, *RSC Adv.*, 2013, **3**, 13059.

Controlled synthesis of three-dimensional V_2O_5/MWCNTs core/shell hybrid aerogel through a mixed growth and self-assembly methodology in a one-pot sol-gel process for high-performance supercapacitor.